JOHANNES KEPLER
UNIVERSITÄT LINZ

Author
Carola Emminger

Host institution
New Mexico State University

Supervisor at host institution
Dr. Stefan Zollner

Temperature dependent investigation of the dielectric function of Ge

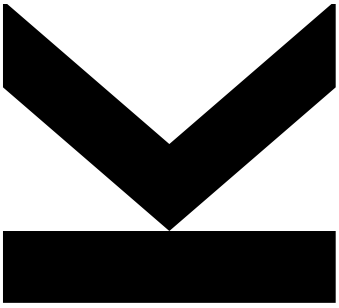

Report

JOHANNES KEPLER UNIVERSITY LINZ
Altenberger Str. 69
4040 Linz, Austria
www.jku.at
DVR 0093696

Contents

Abstract

Spectroscopic ellipsometry measurements were performed to explore the temperature dependence of the dielectric function of bulk germanium (Ge) over a broad spectral range from 0.5 eV to 6.5 eV. In the temperature range from 10 K to 738 K 31 measurements in approximately 25 K steps were taken. The focus of this work lies on the investigation of the E_0 and $E_0 + \Delta_0$ critical points. The dielectric function of Ge was determined using a parametric oscillator model consisting of eight oscillators.

For the energies of all critical points that occur within this spectral range, a shift to lower energies with increasing temperature as well as an increase of the broadening of the E_1, $E_1 + \Delta_1$, E_0' and E_2 critical points was observed. By analyzing the second derivative of the measured dielectric function in terms of photon energy, the critical point parameters of the E_1, $E_1 + \Delta_1$, E_0' and E_2 critical points could be found. Since the peaks of the E_0 critical points are very sharp and narrow the second derivative analysis could not provide reasonable values for the broadening of these critical points. Therefore, for the E_0 and $E_0 + \Delta_0$ further and more precise investigation will be necessary.

Keywords: Spectroscopic ellipsometry, germanium, temperature dependence, critical points, band gap

1 Introduction

Knowledge about the optical constants of germanium (Ge) is of great importance in semiconductor industry since Ge is a material commonly used in applications in electronic devices, such as field-effect transistors (FET), metal-oxide-semiconductor (MOS) integrated circuits, MOS-FET and complementary MOS (CMOS) circuits, just to name a few. There are also numerous applications in optoelectronics, like solar cells or light emitting diodes (LEDs), for instance. It can also be used in alloys together with other materials, such as silicon (Si) or tin (Sn). Examples are $Si_{1-x}Ge_x$ alloys, Si/Ge or Si/SiGe heterostructures. Many of the Ge applications depend on the optical constants, especially the dielectric function (ϵ), which is directly related to the electronic band structure.

Together with Si, Ge is also one of the most thoroughly studied semiconductors. The temperature dependence of the dielectric function of Ge was studied in previous work [1][2] among others, in particular the temperature dependence of the critical points of Ge was studied in [3]. So far, no detailed temperature dependent investigation of the E_0 and $E_0+\Delta_0$ critical points has been published. Therefore, the focus of this work lies on the precise measurement and analysis of these critical points.

Critical points are related to structures in the spectra of the optical constants of semiconductors. In other words, they occur as peaks (or shoulders) in the spectra of the real and imaginary parts of complex dielectric function. These critical points regard to energy differences between the valence and conduction band at certain regions in the Brillouin zone, where the critical point at the Γ-point, the center of the Brillouin zone, is known as E_0. In the case of fine structure, i.e. spin-orbit splitting Δ_0, there is also a second critical point denoted as $E_0 + \Delta_0$. The dielectric function and therefore also the critical points are dependent on temperature, i.e. they shift to lower energies as the temperature increases, which is also called red-shift [1].

For analyzing the data, a parametric oscillator model using eight oscillators described in [4] was applied to find the dielectric function of the bulk Ge. The second derivative of the dielectric function gained by a point-by-point fit of the data with respect to photon energy was calculated in order to determine the critical point parameters.

2 Spectroscopic Ellipsometry

Ellipsometry is a contact free optical measurement technique used to determine, for example, the thickness of a thin film or the dielectric properties, such as the complex refractive index or the complex dielectric function, of organic as well as inorganic samples. Furthermore, the influence of quasiparticles, such as phonons, plasmons and excitons, on the dielectric function can be examined. If ellipsometric data is taken over a wide range of photon energy, it is denoted as *spectroscopic ellipsometry*.

The challenge of ellipsometry lies not in the measurement itself, which is in principle not very complicated, but rather in the relatively complex analysis of the measured data, which requires knowledge and difficult (many particle) modelling. In the past decades, several theoretical models as well as data analysis software have been evolved and promoted ellipsometry to become a commonly used measurement technique in material science and surface analytics. These developments have made it possible to achieve very accurate results within a reasonable time.

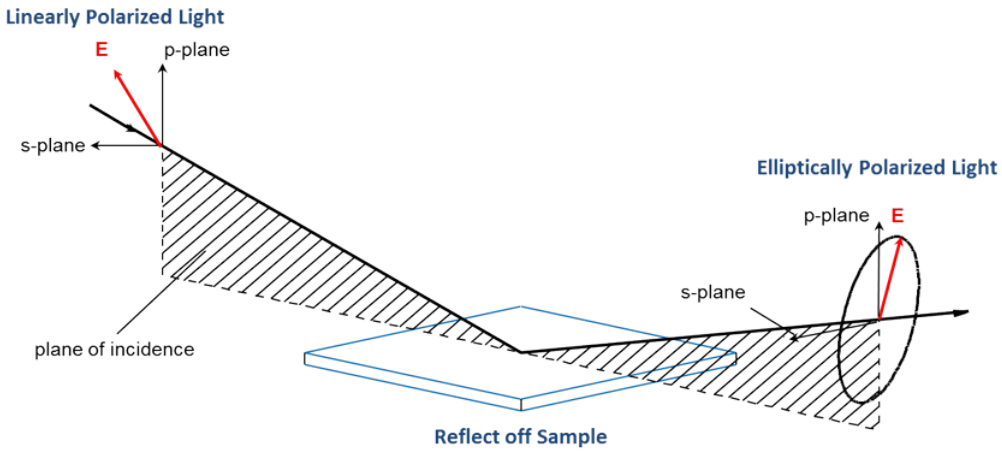

Figure 1: Principle of ellipsometry. Linearly polarized light incident on a sample changes its state of polarization after reflection to elliptically polarized. [www.jawoollam.com/resources/ellipsometry-tutorial/ellipsometry-measurements]

Light is an electromagnetic wave and is described by its polarization, which can be linearly, circularly or elliptically polarized. The principle of ellipsometry is to determine the change of the polarization state of light before and after reflection on or transmission through a material. As light interacts with a

medium, it affects the electric dipole moment per unit volume that causes the change of polarization. The general case is elliptically polarized light, which is the combination of two orthogonal waves that show a difference in phase with respect to each other. The actual value which is measured by an ellipsometer is the change of the p- and s-components of the electromagnetic wave, which are the parts of the light vector in plane (p) and perpendicular (s) to the plane of incidence, as can be seen in figure 1. This can be expressed by the ratio

$$\rho = \frac{r_p}{r_s}, \tag{1}$$

where r_p is the complex reflectivity of the sample for p-polarized and r_s for s-polarized light. They are also known as the Fresnel reflection coefficients and are defined as

$$r_p = \frac{E_p^r}{E_p^i} \tag{2}$$

and

$$r_s = \frac{E_s^r}{E_s^i}. \tag{3}$$

The superscript r stands for *reflected* and i stands for *incident*. That means that the reflection coefficients are defined as the ratios between the reflected and incident field components. The squared absolute value of r_p is equal to the reflectance R_p for p-polarized light

$$R_p = |r_p|^2 = \left| \frac{\tilde{n}^2 \cos\theta - \sqrt{\tilde{n}^2 - \sin^2\theta}}{\tilde{n}^2 \cos\theta + \sqrt{\tilde{n}^2 - \sin^2\theta}} \right| \tag{4}$$

and the squared absolute value of r_s for s-polarized light is

$$R_s = |r_s|^2 = \left| \frac{\cos\theta - \sqrt{\tilde{n}^2 - \sin^2\theta}}{\cos\theta + \sqrt{\tilde{n}^2 - \sin^2\theta}} \right|, \tag{5}$$

where θ is the angle of incidence and $\tilde{n}$ is the complex reflective index. The equations (4) and (5) are known as the Fresnel formulas and they are related to the phase difference Δ and the amplitude component Ψ as

$$\rho = fracr_p r_s = \tan(\Psi)\, e^{i\Delta}. \tag{6}$$

There exist several different types and setups of ellipsometers, which are distinguished by the arrangement of the optical elements. For this work, a rotating analyzer ellipsometer in a so-called *PCSA*-setup was used, which is described in principle in figure 2, if one would remove the second (optional) compensator placed after the sample. The electromagnetic radiation which is emitted by the light source first gets linearly polarized by a polarizer and then passes a compensator. Therefore, the polarization state of the light before it reaches the sample surface is known. After reflection by the sample it travels through an analyzer (which is a second polarizer) that is rotatable and again measures the state of polarization. An additional compensator after the sample as shown in figure 2 was not used, but would be also a common option for an ellipsometric setup. Via the equations (6) the quantities Ψ and Δ can be determined and by the use of a software based on theoretical models, the optical constants can be calculated.

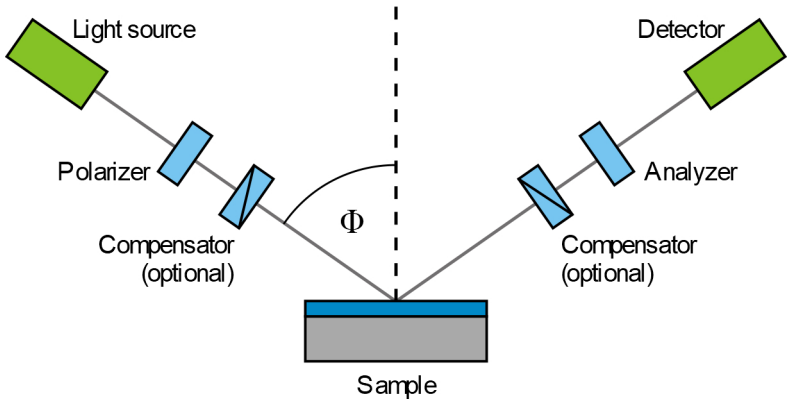

Figure 2: Schematic setup of an ellipsometer: Electromagentic radiation emitted by a light source goes through a polarizer, an optional compensator, gets reflected by a sample and then again goes through an optional compensator and a second polarizer (analyzer). A detector measured the intensity of the light and converts it to an electronic signal. [en.wikipedia.org/wiki/Ellipsometry]

Samples which are investigated by ellipsometry should be as clean and as smooth as possible. A rough surface can cause scattering and depolarization, which makes the analysis of the ellipsometric data difficult. Variations in the thickness of the overlayers of a layer system can also cause problems. To avoid such problems, different kind of cleaning techniques are used in order to remove contaminations.

3 Theory

The electronic band structure of a semiconductor, as shown in figure 3 for Ge, describes the energy dispersion with respect to the wavevector **k**. It is separated into two energy bands: the valence band below and the conduction band above the band gap. In a semiconductor, the Fermi level lies in the middle of the band gap, which means that in the ground state all electrons are in the valence band and the conduction band is empty. Doping can shift the Fermi energy and therefore a semiconducting material can be influenced with regard to its as electrical properties. Semiconductors can show either a direct or an indirect band gap. In the case of a direct band gap semiconductors, such as gallium arsenide (GaAs), for instance, the minimum of the conduction band and the maximum of the valence band both occur at the Γ-point, the center of the Brillouin zone. Examples for indirect band gap semiconductors are Si and Ge, whose band structure is shown in figure 3.

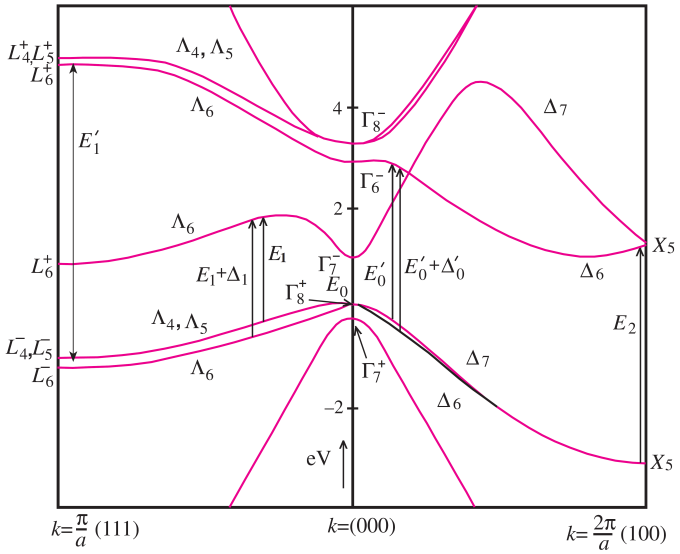

Figure 3: Band structure of germanium showing transitions according to critical points [5]

The crystal structure of a semiconductor influences the shape of the Brillouin zone and therefore the electronic and optical properties. Both materials, Si as well as Ge, are members of the carbon group, which is the group with number 14 in the periodic table. In the field of semiconductors, it is also known as Group IV. Materials of this group show the same crystal structure as diamond, which is a face-centered cubic lattice having four additional atoms within in the unit cell. In group theory, this kind of crystals belong to the O_h^7 (or Fd3m) point group.

3.1 Optical Properties

The complex dielectric function

$$\epsilon(\omega) = \epsilon_1(\omega) + i\epsilon_2(\omega), \tag{7}$$

where ω is the frequency of the photon, describes the interaction of the material with light. The complex dielectric function and the complex refractive index

$$\tilde{n} = n + i\kappa \tag{8}$$

are related to each other as

$$\epsilon(\omega) = (\tilde{n})^2 . \tag{9}$$

When light travels through a material between the points $\mathbf{r}_1$ and $\mathbf{r}_2$ its intensity gets weakened according to the law by Lambert and Beer

$$I = I_0 e^{-\alpha|\mathbf{r}_2 - \mathbf{r}_1|}, \tag{10}$$

where I_0 is the intensity of the light in vacuum and α is called the absorption coefficient of the medium. The imaginary part κ of the complex refractive index, also known as the extinction coefficient, is related to absorption via

$$\alpha = \frac{4\pi\kappa}{\lambda_0}, \tag{11}$$

where λ_0 is the wavelength of the incident light. Due to the relation between (7) and (8), the real part ϵ_2 of the dielectric function is related to the absorption of the material.

3.2 Excitons - Electron-Hole Interaction

As an electron in the valence band gets excited to the conduction band, an electron hole, which is treated like a positively charged particle, remains in the valence band. This results in an electron-hole pair, also known as exciton, due to Coulomb interaction between these two charges. An exciton is a quasi-particle and can be described via a two-particle picture.

In general, two limiting cases of excitons are distinguished. Weakly bound electron-hole pairs are called Wannier-Mott excitons and occur in most semiconductors because the valence electrons weaken the Coulomb interaction by screening due to the large dielectric constant. If the binding energy between the electron and the hole is strong, it is known as a Frenkel exciton. More detailed information about excitons can be found in [5], for example. Electron-hole interaction affects the energy spectrum and optical properties of a semiconductor.

3.3 Critical Points

Critical points occur as peaks or shoulders in the spectrum of the imaginary part of the dielectric function, where the joint density of states shows singularities, called Van Hove singularities. By defining $E_{CV} = E_C - E_V$ the joint density of states can be written as [5]

$$D_j(E_{CV}) = \frac{1}{4\pi^3} \int \frac{dS_k}{|\Delta_k(E_{CV})|}, \tag{12}$$

where S_k is the energy surface where $E_{CV}0$ is constant. Therefore, a Van Hove singularity occurs when $|\Delta_k(E_{CV})|$ in (12) vanishes. That means that a transition takes place where the difference of the k-vectors is equal to zero.

Different kinds of Van Hove singularities are distinguished for one-, two- and three-dimensional space. In other words, Van Hove singularities can occur in the form of minima, maxima or saddle points. The classification of the singularities depends on the number of negative coefficients α_i for $i = 1, 2, 3$ in the expansion of $E(\mathbf{k})$ about a critical point

$$E(\mathbf{k}) = E(0) + \alpha_1 k_1^2 + \alpha_2 k_2^2 + \alpha_3 k_3^2 + \ldots \tag{13}$$

for $\mathbf{k}$=0 [5]. Four different types of Van Hove singularities for three dimensions can be distinguished, namely M_0, M_1, M_2 and M_3 critical points. In the case of no negative α_i's, the critical point is a M_0 critical point according to a minimum in the interband separation, i.e. the energy with respect to the wave vector. Saddle points correspond to either a M_1 or M_2 critical point and a maximum to the M_3 critical point. For a three-dimensional M_0 critical point, for instance, the imaginary part of the dielectric function shows a square root dependence on energy for energies above the critical point energy. An example for such a point would be the onset at the band gap energy (the E_0 critical point) in the spectrum of the imaginary part of the dielectric function of Ge, as can

be seen in figure 4 for an energy of about 0.88 eV. The critical point E_1 and $E_1 + \Delta_1$, on the other hand, are examples for two-dimensional critical points M_1, having a logarithmic dependence on energy. An example for a mixture of a three-dimensional M_0 and a M_1 critical points was used in [1] for the E_0' and $E_0' + \Delta_0'$ critical points.

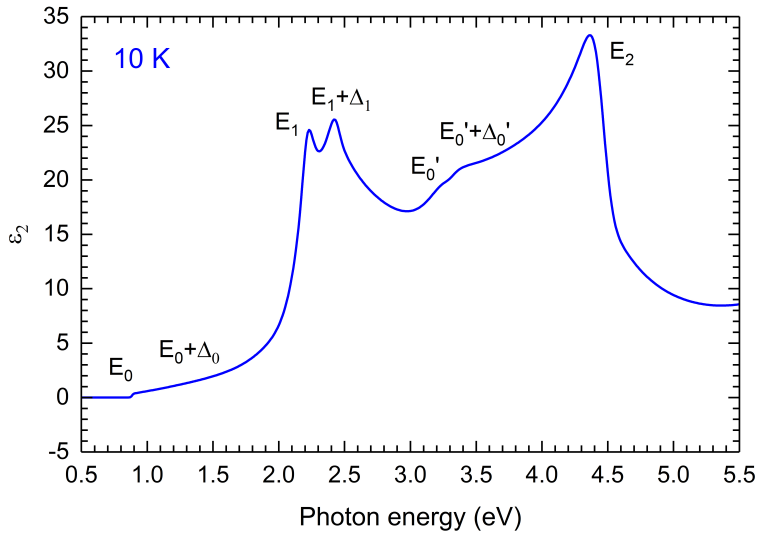

Figure 4: Imaginary part of the dielectric function of germanium at 10 K showing several critical points.

In the spectrum of the real part of the dielectric function these critical points can be identified as peaks or shoulders. The critical point that is related to transitions at the center of the Brillouin zone, i.e. the band gap of a material, is denoted as E_0. For the indirect band gap semiconductor germanium there is also spin-orbit splitting denoted as Δ_0 occurring at the Γ-point which results in two peaks in the spectrum of the dielectric function, namely E_0 and $E_0 + \Delta_0$. In figure 4 the E_0 and $E_0 + \Delta_0$ critical points are shown alongside the other critical points E_1 and $E_1 + \Delta_1$, E'_0 and $E'_0 + \Delta'_0$ and E_2. The E_1 and $E_1 + \Delta_1$ critical points result from transitions along the Λ direction, E'_0 and $E'_0 + \Delta'_0$ along the Δ direction and E_2 corresponds to the X-point, as can be seen in figure. For the rest of this report, the E'_0 and $E'_0 + \Delta'_0$ are considered to behave like one single critical point E'_0, since the spin-orbit splitting can hardly be perceived at higher temperatures than 10 K.

In the case of linear optics, i.e. when the strength of an external field is weak,

the dielectric function $\epsilon(\omega)$ describes a linear response to an external field. Linear response functions satisfy the Kramers-Kronig relations, which are

$$\epsilon_1(\omega) = 1 + \frac{2}{\pi} CP \int_0^\infty \frac{\omega' \epsilon_2(\omega')}{\omega'^2 - \omega^2} d\omega' \tag{14}$$

for the real part and

$$\epsilon_2(\omega) = -\frac{2\omega}{\pi} CP \int_0^\infty \frac{\epsilon_1(\omega')}{\omega'^2 - \omega^2} d\omega' \tag{15}$$

for the imaginary part of the dielectric function. The value CP is the socalled Chauchy principle value (or just principle value) of the integral. The Kramers-Kronig relations connect the two parts, so if, for example, the real part is known, the imaginary part can be calculated.

Excitations of a semiconductor by excitons or phonons can be expressed by Lorentz oscillators. It describes basically an electron bound to the core of an atom which gets excited to harmonic oscillations by an external electric field. Therefore, the equation for a Lorentz oscillator can be derived from the equation of motion due to a damped harmonic oscillator

$$m\frac{d^2x}{dt^2} + m\gamma\frac{dx}{dt} - m\omega_0 x = -qF_0 e^{i\omega t}, \tag{16}$$

where m is the mass of the electron, γ is a damping parameter, ω_0 is the eigenfrequency of the undamped harmonic oscillator, q is the charge of the electron, F_0 is the amplitude and ω the frequency of the driving external field. The solution of this equation of motion can be found as

$$x(t) = -\frac{q}{m}\frac{F_0 e^{-i\omega t}}{\omega_0^2 - \omega + i\gamma\omega}. \tag{17}$$

The theory of Lorentz oscillators can be applied to the polarization of a material, because the displacement of charges are directly related to the polarization. Therewith, a similar equation for the dielectric function can be found

$$\epsilon(\omega) = \epsilon_0 \left(\frac{\omega_p^2}{\omega_0^2 - \omega + i\gamma\omega} \right). \tag{18}$$

with

$$\omega_p^2 = \frac{Nq^2}{\epsilon_0 m}, \tag{19}$$

where N is the number of charges per unit volume and ϵ_0 is the permittivity of vacuum. Equation (18) can be separated in a real and an imaginary part, respectively.

As it is explained in [1], the dielectric function with respect to photon energy can be modelled as

$$\epsilon(\omega) = C - Ae^{i\phi}(\omega - E_g - i\Gamma)^{\mu}, \tag{20}$$

where A is the amplitude, E_g is the critical point energy, Γ is the broadening parameter, and ϕ is the excitonic phase angle. The constant C is the non-resonant background due to other critical points [3] and vanishes for the second derivative, respectively.

3.4 Parametric Oscillator Model

For anaylzing the ellipsometric data, the parametric oscillator model described in [4] is applied (the results are shown in section 5). The optical constants of a semiconductor can be derived from the data by using this model that takes advantage from being Kramers-Kronig consistent.

In principle, the model consists of a number of oscillators corresponding to critical point structures in the spectra of the optical constants. These oscillators occur at certain photon energies (the critical point energies) and are defined by a set of parameters, including a broadening and an amplitude.

All in all, the set of parameters consists of 13 different parameters which all can be varied in order to find the best fit to the data. An oscillator j at an center energy $E_{j,C}$, having a broadening B_j and a center amplitude A_j, spans the range from the lower energy $E_{j,L}$ to the higher energy $E_{j,U}$. It is connected to the oscillator i to the left and k to the right side. Here, it has to be noted that i, j and k do not necessarily have to be placed "next to each other" in the spectrum of the optical constants. There can be another critical point between them, for example. The other fitting parameters are the upper and lower mid-positions, upper and lower mid-amplitudes and upper and lower second order polynomial factors. Another parameter is the amplitude discontinuity, which is related to the joint density of states at the critical point, although it is mentioned in [4] that within this model it is mainly a fitting parameter and does not really have

a physical meaning.

In this work, eight oscillators are used, one for each critical point E_0, $E_0 + \Delta_0$, E_1, $E_1 + \Delta_1$, E_0', E_2, another one for the low and broad peak occurring between 5.5 eV and 6 eV and a "dummy" critical point lying outside the range of the measured ellipsometric data (above 7 eV), which is necessary to sustain Kramers-Kronig consistency. Otherwise the model would not provide reasonable results.

4 Measurement of the Dielectric Function of Germanium

Using an ellipsometer [6] at an incident angle of 70° the pseudodielectric function of the Ge sample was measured over a wide spectral range from 0.5 eV to 6.5 eV for 31 different temperatures between 10 K and 738 K. In figure 5 the experimental setup can bee seen, showing the ellipsometer and the cryostat which was used to create an ultra-high vacuum (UHV) environment for the Ge sample.

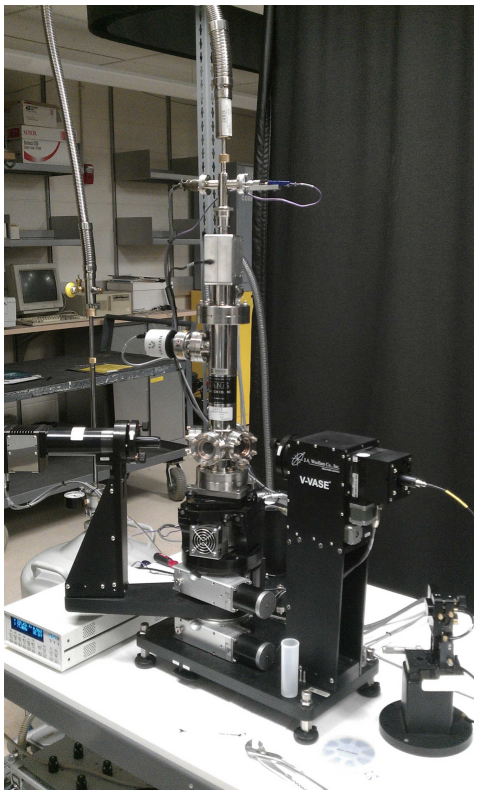

Figure 5: Ellipsometer and cryostat [ellipsometry.nmsu.edu]

To cool the sample down below room temperature, liquid nitrogen (having its boiling point at 77 K) and liquid helium (4 K) were used as cryogens. In the background of figure 5 the tank containing liquid nitrogen connected via an isolated hose to the top of the cryostat can be seen. Two thermocouples were applied in order to measure the temperature. While one was attached directly to the sample surface to accurately show the temperature of the sample itself, the other one measured the temperature of the cryostat. We observed a

difference between the values shown by the two thermocouples, i.e. the temperature that was set and that of the sample, which increases with distance to room temperature. For the lowest temperature that could be reached by using liquid helium, the actual temperature of the sample was above that of the gas, namely 10 K instead of 4 K. For the liquid nitrogen measurement we observed a temperature of 20 K instead of 77 K. However, we trust the measurement of the thermocouple attached to the sample surface to provide the actual temperature of the sample accurately. For temperatures between 82 K and room temperature, a heater connected to the cryostat had to be activated in addition to the liquid nitrogen flow. To keep the temperature in the vacuum chamber stable, the correct amount of nitrogen flow had to be found. To further heat the sample up to temperatures above room temperature the heater was simply set to the wanted temperature. For each measurement we had to wait for the temperature to become stable. Once at an equilibrium, the sample temperature was found to be relatively stable and only varied about $\pm 1\ K$.

On the surface of the bulk Ge substrate a native GeO_2-layer forms as the sample is exposed to air. Together with surface roughness the oxide layer influences the measurement, i.e. it can cause depolarization which makes data interpretation more difficult. Therefore, we tried to minimize the thickness of the oxide layer. To reduce the thickness of the oxide layer and to remove surface contamination, a cleaning procedure was performed prior to the measurements. First, the sample was put into ultra pure water and an ultrasonic bath for 20 minutes, then it was put into isopropyl alcohol and again an ultrasonic bath for another 20 minutes. The next step was to perform an ozone clean, which increased the oxide layer thickness again. After the ozone clean which lasted for 30 minutes the procedure using ultra pure water, isopropyl alcohol and the ultrasonic bath was repeated.

Immediatly after the process of cleaning, the Ge probe was fixed to a copper cold finger using metal clamps covered by a gold-coated copper radiation shield and put into a cryostat, where an ultra high vacuum (UHV) was produced. The vacuum is needed to ensure that the sample does not get contaminated and that the thickness of the GeO_2-layer is stable over the whole temperature range. In order to degas the chamber and the sample, the cryostat was heated up to 700 K and kept at that temperature for several hours. The base pressure of the vacuum system was of the magnitude of 10^{-8} Torr, which is necessary to avoid the growth of ice on the sample surface.
In figure 6 the variation of the GeO_2-layer thickness is shown with respect to temperature. The thickness of the oxide layer varies between 8.5 Åand 11 Å. The reason for the thicker layer at 10 K might be condensation of ice on the

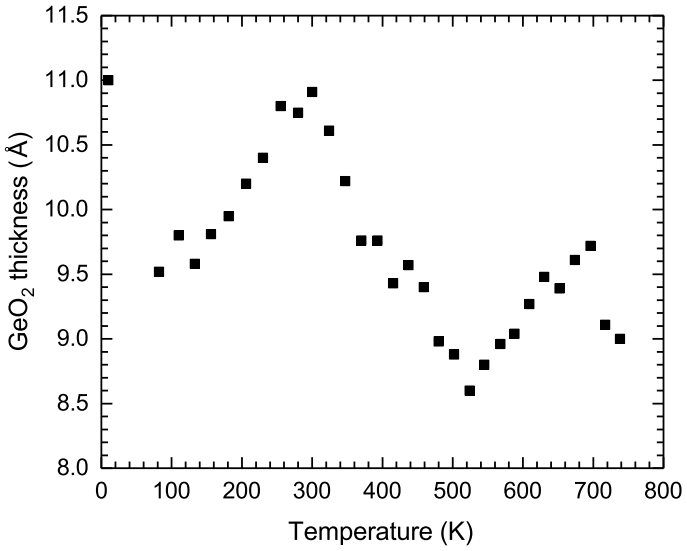

Figure 6: Thickness of the GeO_2-layer with respect to temperature determined with an ellipsometric measurement (9.7 ± 0.6 Å).

top of the sample, which can happen at such low temperatures. Over all, the thickness is very stable over the whole temperature range, showing an average of 9.7 ± 0.6 Å.

It was not possible to take the measurements over the whole spectral range from 0.5 eV to 6.5 eV at once, since the light source and the corresponding glass fibers only work in a certain region of the spectrum. For photon energies between 0.5 eV and 3 eV, i.e from the visible range to the infrared (IR) range, a quartz tungsten halogen (QTH) light source was used and a suitable glass fiber for this energy range. In the range from 0.7 eV up to energies in the ultraviolet (UV) range, i.e. higher than 3 eV, a xenon lamp was chosen as light source. Consequently, for each temperature two measurements had to be taken. After changing the light source, the lamp as well as the fiber had to be aligned and calibrated, respectively. The overlap for each each measurement pair is 2.3 eV (from 0.7 eV to 3 eV). Over all, the measurements at the two different photon energy ranges were found to be in good agreement and could be merged for each temperature.

In order to achieve appropriate accuracy a step size of 10 meV was used for all measurements except for the investigation of the E_0 and $E0 + \Delta_0$ critical points at low temperatures, where a smaller step size was chosen. Several

measurements at 10 K were taken for step sizes of 10 meV, 5 meV, 1 meV and 0.5 meV. Additionally, the minimum slit width of the monochromator of the ellipsometer was set to 1 mm instead of 2 mm, because it influences the resolution and therefore the broadening of the measured data. For example, for a measurement at an energy of 0.878 eV and a slit width of 2 mm the resolution due to the instrument is $\Delta E = 5\ meV$, while for a slit width of 1 mm it is only $\Delta E = 2.5\ meV$.

For each measurement, the sample was aligned prior to starting the measurement to prevent inaccuracies due to thermal deformations. The windows of the cryostat, which consist of quartz glass, can also have an impact on the measurement and have to be considered. To eliminate this problem, a calibration prior to the measurement was performed.

Two different kinds of detectors are used for different energy ranges, an InGaAs detector in the infrared region, and for the rest of the spectrum, a Si CCD detector. The two detectors get switched automatically at a defined wavelength. In addition, there are three wavelength dependent gratings in the monochromator which have to be changed at certain energies. The switches of the gratings is performed automatically by the system as well. The switches of the detectors and gratings can be visible in the measured spectra if the monochromator, the light beam or the detectors are not calibrated perfectly.

5 Data Analysis

The measured pseudodielectric functions $\langle\epsilon\rangle$ for the Ge-GeO_2 layer system for different temperatures are shown in figure 7.

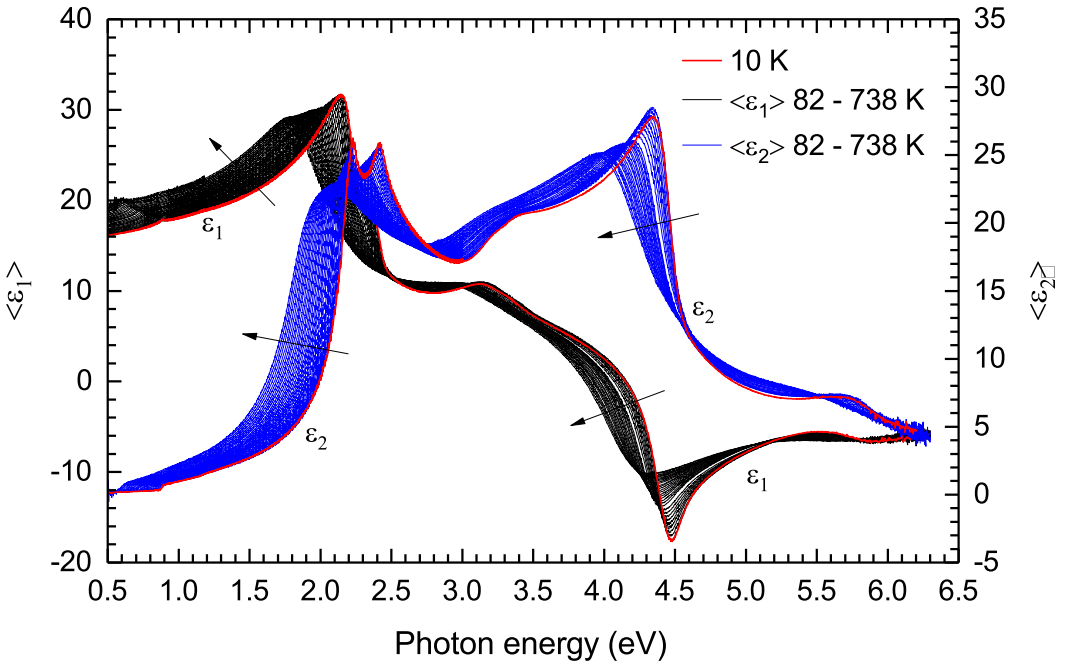

Figure 7: Pseudodielectric function of bulk Ge. Temperature dependence of the real (ϵ_1, black) and imaginary (ϵ_2, blue) parts of the dielectric function from 10 K to 738 K. The arrows indicate the temperature direction from the lowest (10 K, red) to the highest (738 K) temperature.

The optical constants for GeO_2 were taken from literature [7] and were supposed to be temperature independent, so that for each measurement the dielectric function of Ge could be determined by using a fitting procedure in two main steps using a parametric oscillator model described in [4]. This model imposes Kramers-Kronig consistency between the real and imaginary parts of the dielectric function. With respect to our spectral range eight oscillators were used, each of them occuring at a certain energy and described by a broadening Γ, an amplitude A and other additional parameters as described in [4] and in the previous section.

The first step was to determine the thickness of the GeO_2-layer as a function of temperature as shown in figure 6 and to adjust the parameters of the model.

In the second step, the GeO_2-layer thickness was fixed at the value determined in the first step and the oscillator parameters were varied until the best fit to the data was found. This procedure was applied to all 31 measurements. The resulting real (ϵ_1) and imaginary (ϵ_2) parts of the dielectric function of Ge for each temperature is shown in figure 8.

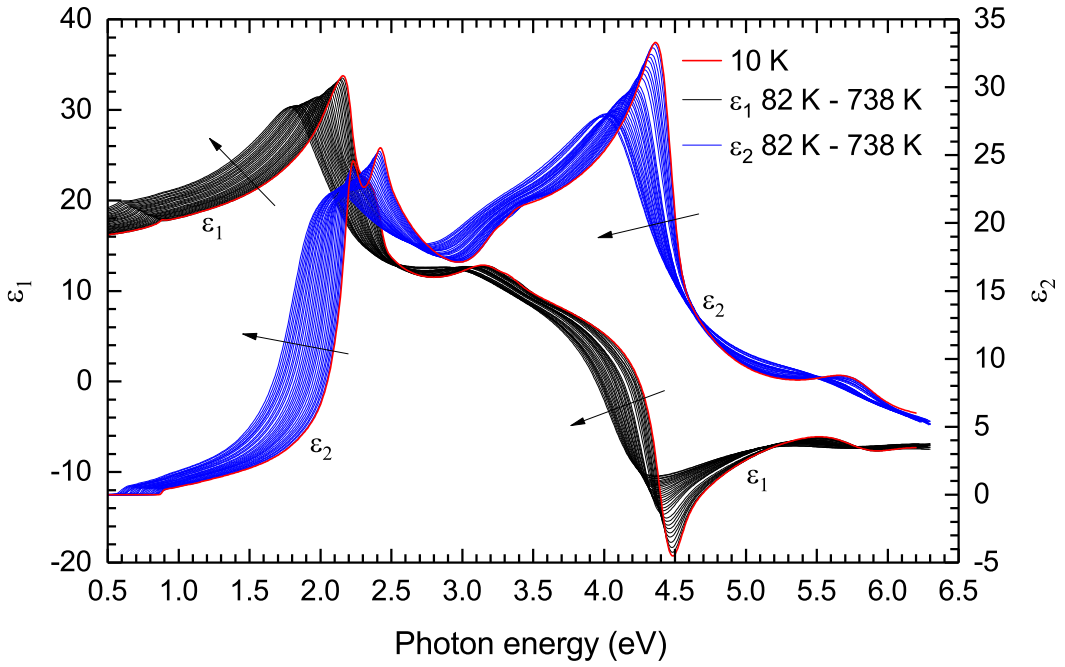

Figure 8: Temperature dependence of the real (ϵ_1, black) and imaginary (ϵ_2, blue) parts of the dielectric function of bulk Ge from 10 K to 738 K. The arrows indicate the temperature direction from the lowest (10 K, red) to the highest (738 K) temperature. Data fitted using the parametric oscillator model.

The red curves in figure 7 show the real and imaginary parts of the pseudodielectric function at 10 K to be significantly lower than expected as it does not follow the trend of the rest of the data sets. The reason for this is the condensation of a thin ice layer at this very low temperature, as mentioned in the previous section. After applying the fitting procedure described above, the dielectric function at 10 K reaches reasonable values since the thicker oxide layer thickness has been considered.

Furthermore, it can be noticed that the structures in the spectra of the dielectric functions and therefore the critical points are red-shifted, i.e. shifted to

lower energies, with increasing temperature, as was expected. This red-shift has two contributions [2]. First, the thermal expansion of the lattice together with a change of electron energies with volume causes a shift towards lower energies. The second contribution comes from the renormalization of the electron energies due to electron-phonon interactions [2].

In the experiment, the total energy shift is measured, i.e. the sum of the contributions due to the thermal expansion and renormalization due to the electron-phonon interaction. The latter one can be described by the Bose-Einstein occupation factor as

$$E_{renorm}(T) = a' - b' \left[1 + 2/\left(e^{\theta'_B/T} - 1\right)\right], \tag{21}$$

where a' is the unrenormalized transition energy, b' the electron-phonon coupling strength and $k\theta'_B$ the effective phonon energy.

The temperature dependence of the total energy shift, including the thermal expansion contribution, can also be expressed via a Bose-Einstein relation

$$E(T) = a - b \left[1 + 2/\left(e^{\theta_B/T} - 1\right)\right]. \tag{22}$$

For the broadening of the critical points a similar expression using the Bose-Einstein occupation factor can be found [1][3]

$$\Gamma(T) = \Gamma_1 + \Gamma_0 \left[1 + 2/\left(e^{\theta_B/T} - 1\right)\right]. \tag{23}$$

Again, the parameter Γ_0 corresponds to electron-phonon interaction.

5.1 Critical Point Parameters

In order to investigate the critical points the second derivatives $d^2\epsilon_1/d^2$ and $d^2\epsilon_2/d^2$ of the complex dielectric function were calculated and analyzed. For this purpose, a point-to-point fit ofthe dielectric function data was performed and from this fit, the second derivatives were determined. Critical points are represented by certain line shapes and are described by a broadening and an amplitude as described in equations (21)-(23). These parameters can be found by applying analysis based on the Savitzky-Golay coefficients [3] and gives reasonable results for the E_1, $E_1 + \Delta_1$, E'_0 and E_2 critical points.

However, for the E_0 critical point this procedure does not work since the broadening of the E_0 peak is too narrow and hence the second derivative analysis is not sufficient. To analyze the E_0 critical point it might be more sufficient to investigate the data not in direct but rather in reciprocal space using a Fourier transform and study the resulting Fourier coefficients.

In the tables 1 and 2 the parameters with respect to equations (22) and (23) calculated by the second derivative method are listed and compared to the parameters of previous work.

Table 1: Parameters according to the Bose-Einstein occupation factor in equation (22) for the E_0, $E_0 + \Delta_0$, E_1, $E_1 + \Delta_1$, E'_0 and E_2 critical points. The E_0 and $E_0 + \Delta_0$ critical points have been fitted using the parametric oscillator model instead of the second derivative anaylsis method.

	a (eV)	b (eV)	θ_B (K)
E_0	0.948 ± 0.003	0.070 ± 0.004	296 ± 16
$E_0 + \Delta_0$	1.232 ± 0.006	0.050 ± 0.009	213 ± 35
E_1	2.292 ± 0.002	0.059 ± 0.003	198 ± 10
E_1 [3]	2.295 ± 0.002	0.063 ± 0.004	218 ± 14
E_1 [1]	2.33 ± 0.03	0.12 ± 0.04	360 ± 120
$E_1 + \Delta_1$	2.494 ± 0.002	0.064 ± 0.003	213 ± 9
$E_1 + \Delta_1$ [3]	2.494 ± 0.002	0.064 ± 0.003	218 (f)
E'_0	3.34 ± 0.02	0.15 ± 0.02	581 ± 42
E'_0 [3]	3.18 ± 0.02	0.05 ± 0.02	313 ± 107
E'_0 [1]	3.23 ± 0.02	0.08 ± 0.03	484 ± 136
E_2	4.508 ± 0.006	0.044 ± 0.003	169 ± 41
E_2 [3]	4.505 ± 0.006	0.05 ± 0.01	217 ± 41
E_2 [1]	4.63 ± 0.05	0.17 ± 0.06	499 ± 127

In the following sections, the results for the critical point parameters for E_1, $E_1 + \Delta_1$ and E_2 determined by the second derivative analysis are presented. Additionally, the E_0 and $E_0 + \Delta_0$ critical points are discussed.

5.1.1 Results for E_1 and $E_1 + \Delta_1$

In figure 9 the temperature dependence of the E_1 and $E_1 + \Delta_1$ critical point energies is presented. The energies have been determined using the second derivative analysis described in the previous section. The fit to the data has been calculated via equation (22) using the Bose-Einstein occupation factor.

Table 2: Broadening parameters according to the Bose-Einstein occupation factor in equation (23) for the broadening of the E_1, $E_1 + \Delta_1$, E'_0 and E_2 critical points.

	Γ_1 (meV)	Γ_2 (meV)	θ_B (K)
E_1	6 ± 2	25 ± 3	341 ± 34
E_1 [3]	11 ± 1	14.2 ± 0.3	218 ± 14
E_1 [1]	12 ± 9	25 ± 3	376(f)
E_1+Δ_1	14 ± 1	20(f)	250(f)
E_1+Δ_1 [3]	22 ± 3	15.1 ± 0.6	218(f)
E_1+Δ_1 [1]	9 ± 8	43 ± 5	484(f)
E'_0	3.34 ± 0.02	0.15 ± 0.02	581 ± 42
E_2	19 ± 14	53 ± 17	443 ± 41
E_2 [3]	38 ± 2	22.1 ± 0.5	217(f)
E_2 [1]	8 ± 5	69 ± 3	499(f)

In table 1 the parameters of the Bose-Einstein fit for this and for previous work [1][3] can be found. The energies decrease with increasing temperature due to thermal expansion and electron phonon interaction as mentioned above.

A deviation of the fits of this work and [3] can be observed for both critical points. The fits for $E_1 + \Delta_1$ agree at lower temperatures and start to deviate from each other above approximately 420 K. The values of [3] are obviously lower for higher temperatures. For the E_1 critical point, on the other hand, the fit corresponding to [3] shows higher values for temperatures above 140 K while the fit corresponding to [1] shows lower values for higher temperatures and deviates notably at temperatures below 160 K. It is not yet clear where this deviations stem from, although it might be due to the lack of data in the region below 100 K.
The temperature independent spin-orbit splitting Δ_1 showing an average value of 199 ± 2 meV is shown in figure 10. Compared to [3] it is found to be in good agreement despite the deviation of the critical point energies mentioned above. Also, like observed in [3], the values fluctuate more at temperatures above 600 K and Δ_0 is significantly higher than in [1].
The values for the broadening Γ of the E_1 and $E_1 + \Delta_1$ critical points fluctuate more than those for the energies, especially for $E_1 + \Delta_1$. Also, the deviation compared to [1] and [3] is considerable. Nevertheless, it was possible to find a reasonable fit by using equation 23. The values are compared to those of the previous work in table 2.

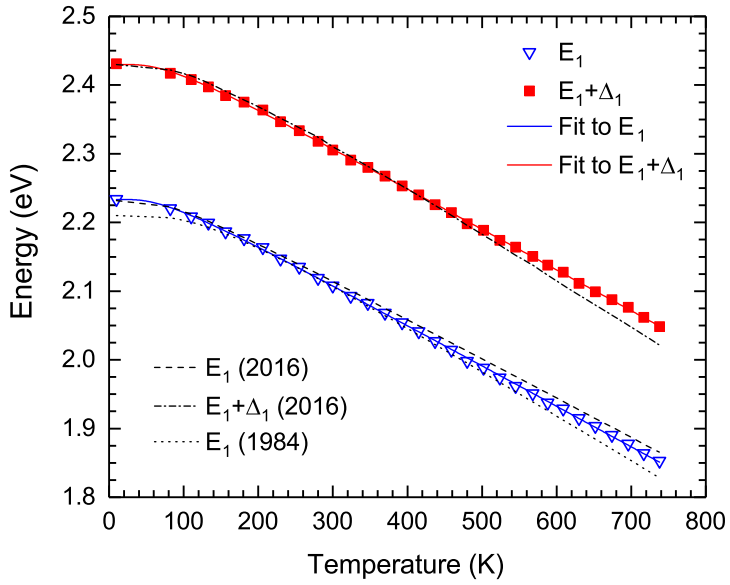

Figure 9: Temperature dependence of E_1 ($\bigtriangledown$) and $E_1 + \Delta_1$(■) critical point energies of bulk Ge. Fit to the data (solid lines) using the Bose-Einstein expression (22). Dashed and dash-dotted lines according to [3], dotted lines according to [1].

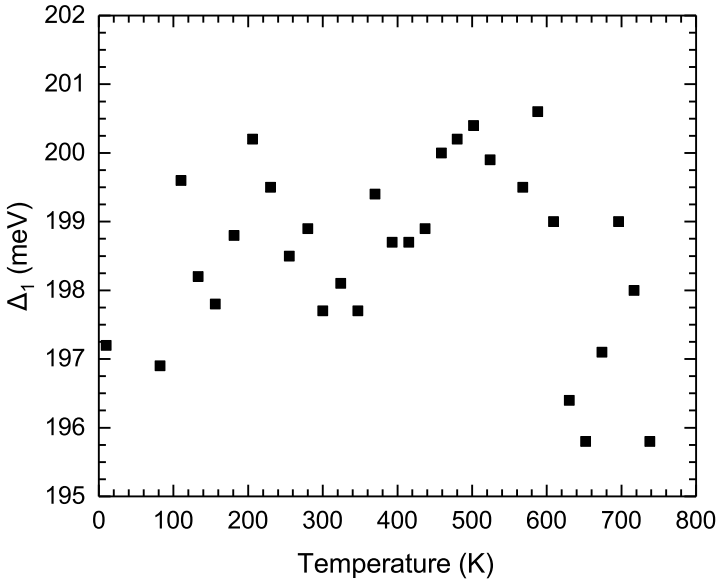

Figure 10: Energy difference Δ_1 between the E_1 and $E_1 + \Delta_1$ critical point energies of bulk Ge due to spin-orbit splitting.

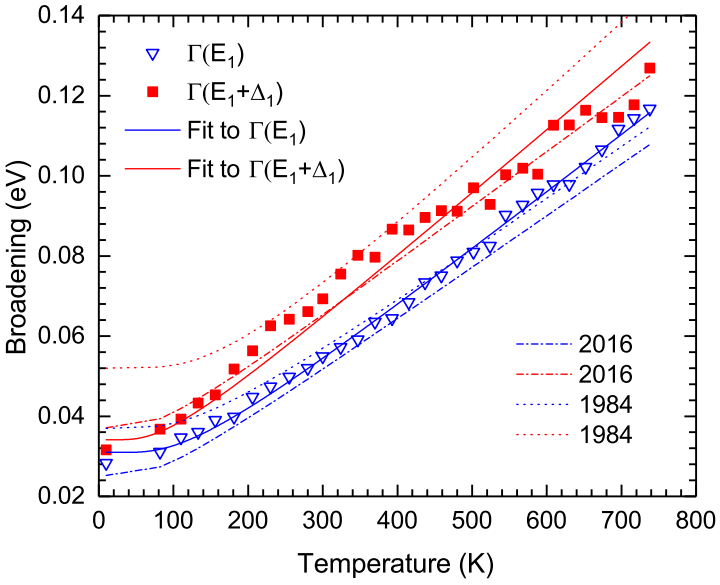

Figure 11: Temperature dependence of the broadening of the E_1 and $E_1 + \Delta_1$ critical points. Fit to the data (solid line) using the Bose-Einstein expression. Dash-dotted line according to [3], dotted lines according to [1].

The amplitudes shown in figure 12 and the phase angles shown in figure 13 show a similar behaviour and comparable values as in [3]. The phase angles are the same for both critical points and compared to [3] they are shifted about 180°, which is consistent with theory.

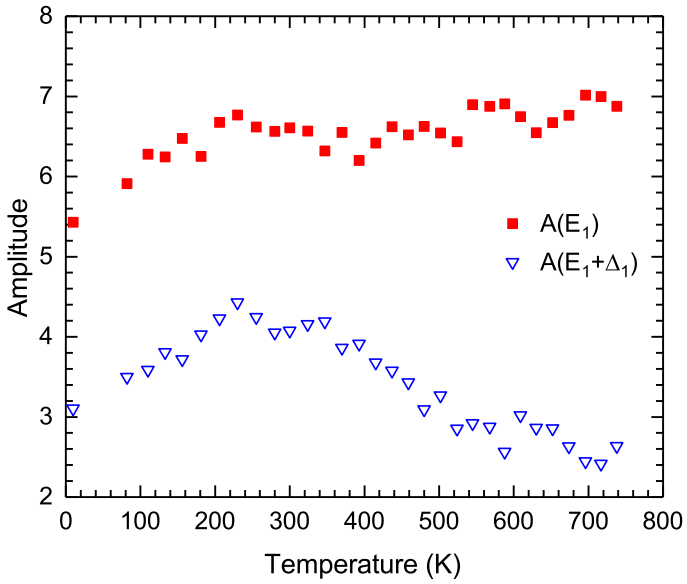

Figure 12: Amplitudes of the E_1, $E_1 + \Delta_1$ and E_2 critical points.

5.1.2 Results for E_2

The results for E_2 critical point parameters are shown in figures 14 to 17. Like for the E_1 and $E_1 + \Delta_1$ critical points, the temperature dependence of the E_2 energies deviates from those in [1] and [3].
The temperature dependence of the amplitudes, the broadening as well as for the phase angles corresponding to the E_2 critical points show a similar behaviour than the parameters in [3]. At temperatures around room temperature, the fit to the values of the braodening are comparable while for lower and higher temperatures the deviation becomes significant.

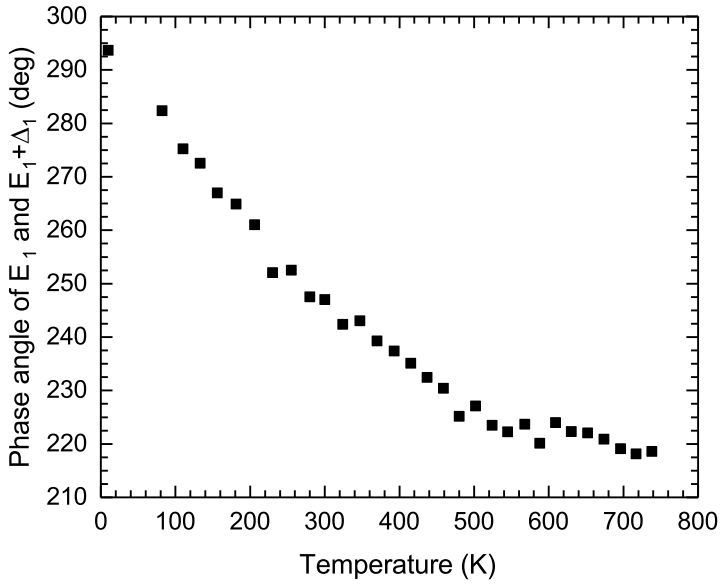

Figure 13: Excitonic phase angle of the E_1 and $E_1 + \Delta_1$ critical points.

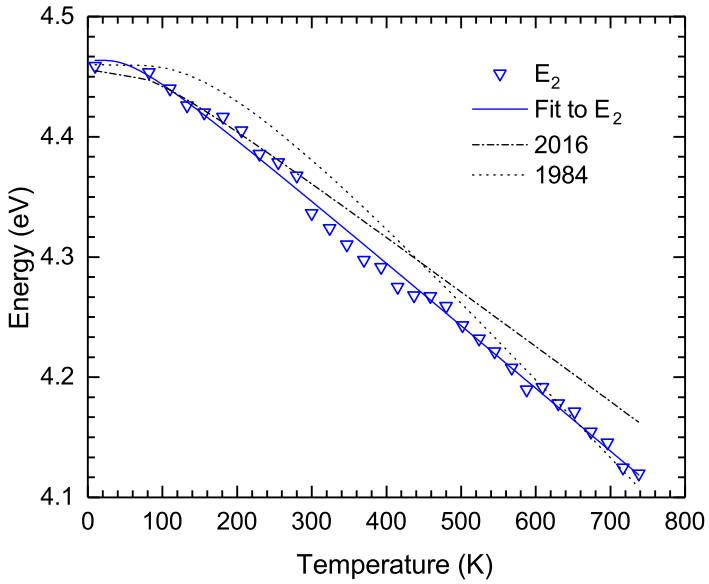

Figure 14: Temperature dependence of the E_2 critical point energies of bulk Ge. Fit to the data (solid line) using the Bose-Einstein occupation factor. Dash-dotted line according to [3], dotted lines according to [1].

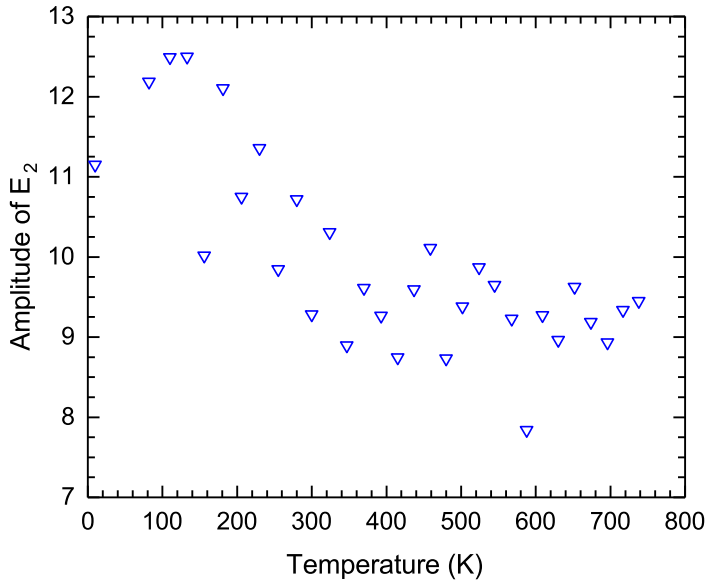

Figure 15: Amplitude of the E_2 critical point.

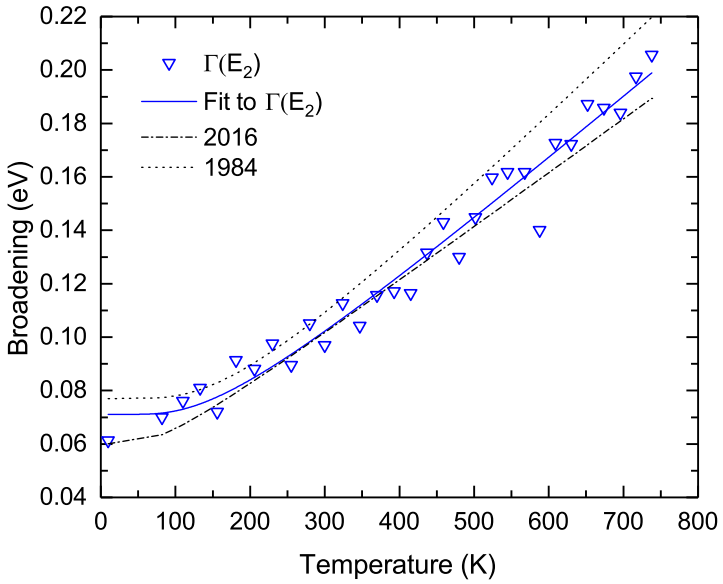

Figure 16: Temperature dependence of the broadening of the E_2 critical point. Fit to the data (solid line) using the Bose-Einstein expression. Dash-dotted line according to [3], dotted lines according to [1].

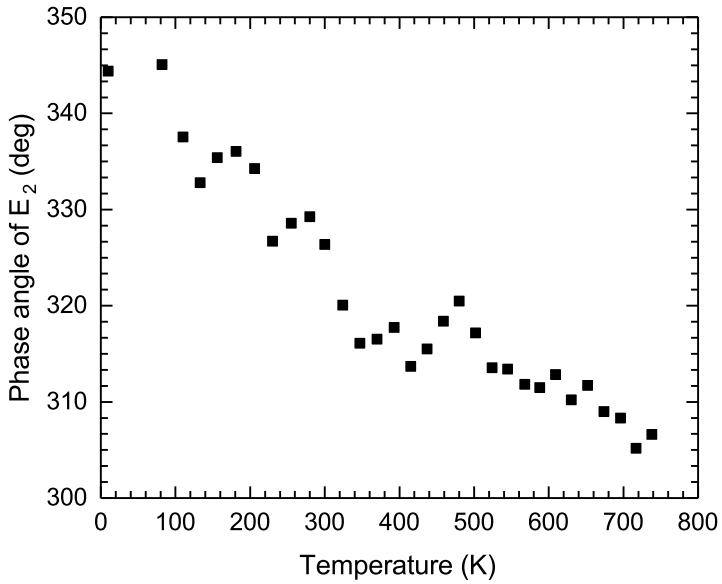

Figure 17: Excitonic phase angle of the E_2 critical point.

5.1.3 Results for E_0 and $E_0 + \Delta_0$

In figures 19 to 22 the real and imaginary parts of the pseudodielectric function are shown in the energy range from 0.5 eV to 1.3 eV including the E_0 and $E_0 + \Delta_0$ critical points at five different temperatures between 10 K and 652 K. The dash-dotted vertical lines indicate the energies of the E_0 critical point and the solid vertical lines those of the $E_0 + \Delta_0$ critical points. These energies were determined using the parametric oscillator model described above.

For temperatures above 650 K the data below 0.6 eV becomes very noisy. The reason for this increaseof noise in the infrared region is supposed to be blackbody radistion. By using a simple iris behind the windows of the cryostat, the noise could be significantly decreases.

For the measurements at room temperature and above a step size of 10 meV and a monochromator slit width of at least 2 mm were used, while at 10 K the step size was set to 1 meV and a slit width minimum of 1 mm was chosen in order to resolve the structures of the E_0 and $E_0 + \Delta_0$ critical points as accurate as possible.

Like for the other critical points occurring at higher energies, a red-shift of

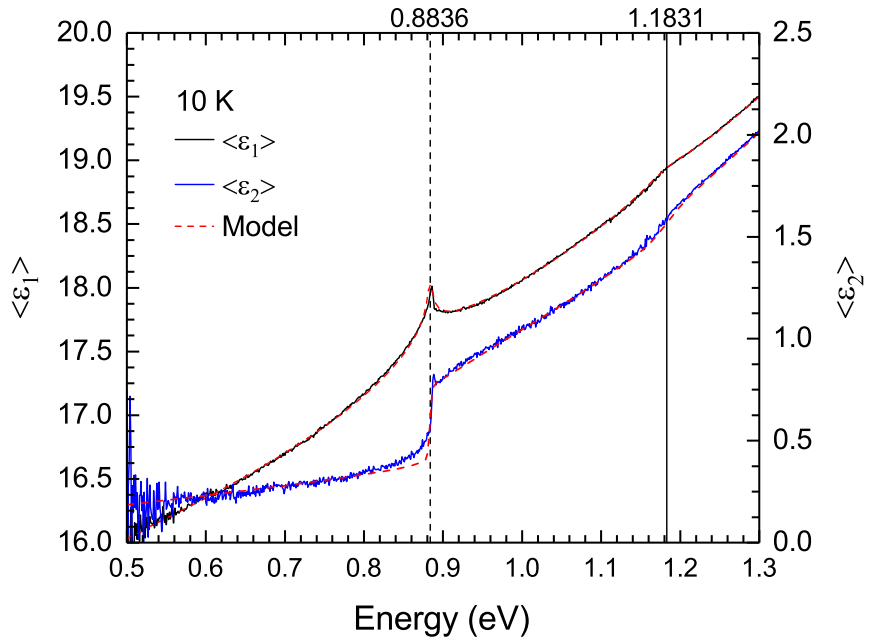

Figure 18: Infrared measurement: Critical points E_0 and $E_0 + \Delta_0$ at the temperature reached by the use of liquid helium, i.e. 10 K. For this measurement, a step size of 1 meV and a slit width minimum of 1 mm were used. The vertical lines indicate the critical point energies of E_0 (dash-dotted) and $E_0 + \Delta_0$ (solid) obtained by a parametric oscillator fit.

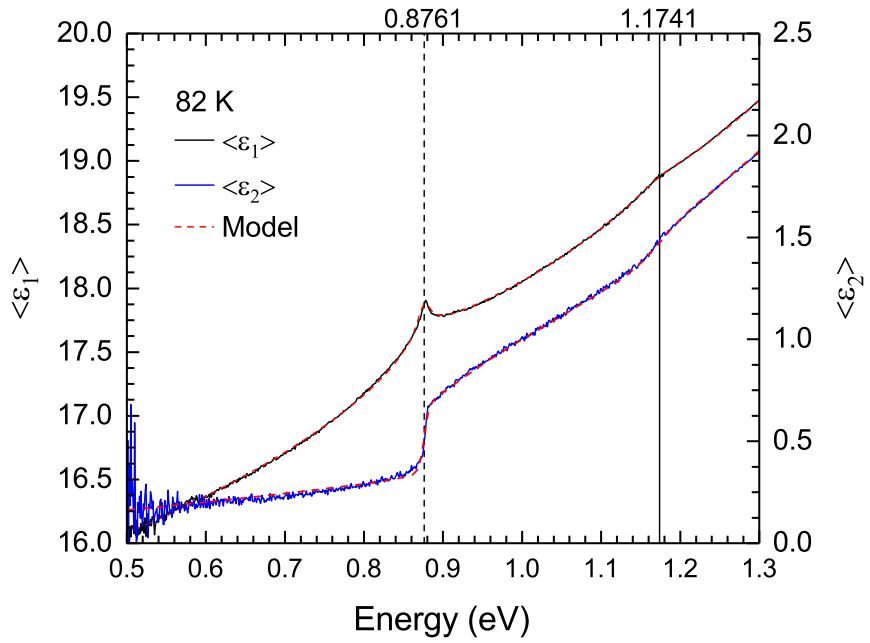

Figure 19: Infrared measurement: Critical points E_0 and $E_0 + \Delta_0$ at the liquid nitrogen temperature, i.e. 82 K. The vertical lines indicate the critical point energies of E_0 (dash-dotted) and $E_0 + \Delta_0$ (solid) obtained by a parametric oscillator fit.

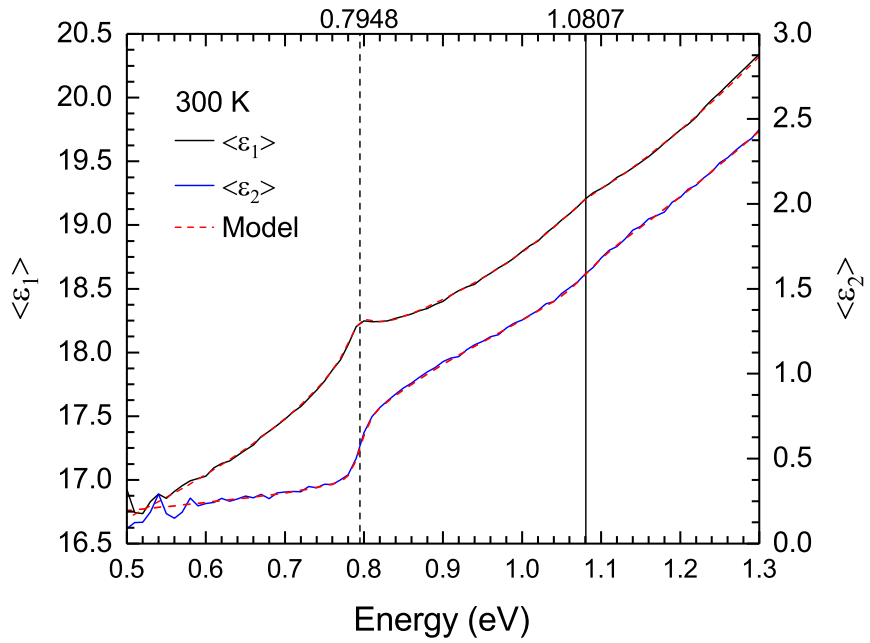

Figure 20: Infrared measurement: Critical points E_0 and $E_0 + \Delta_0$ at room temperature. The vertical lines indicate the critical point energies of E_0 (dash-dotted) and $E_0 + \Delta_0$ (solid) obtained by a parametric oscillator fit.

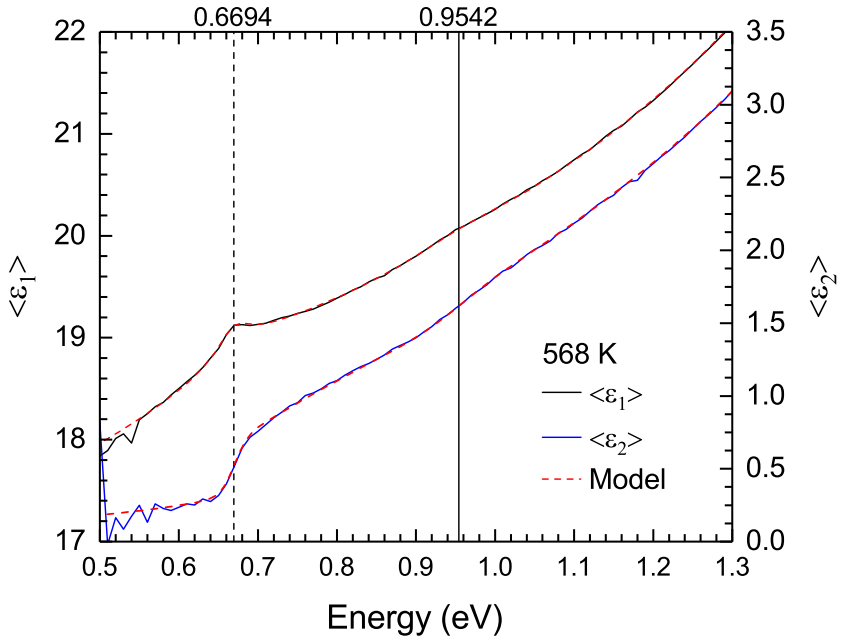

Figure 21: Infrared measurement: Critical points E_0 and $E_0 + \Delta_0$ at 568 K. The vertical lines indicate the critical point energies of E_0 (dash-dotted) and $E_0 + \Delta_0$ (solid) obtained by a parametric oscillator fit.

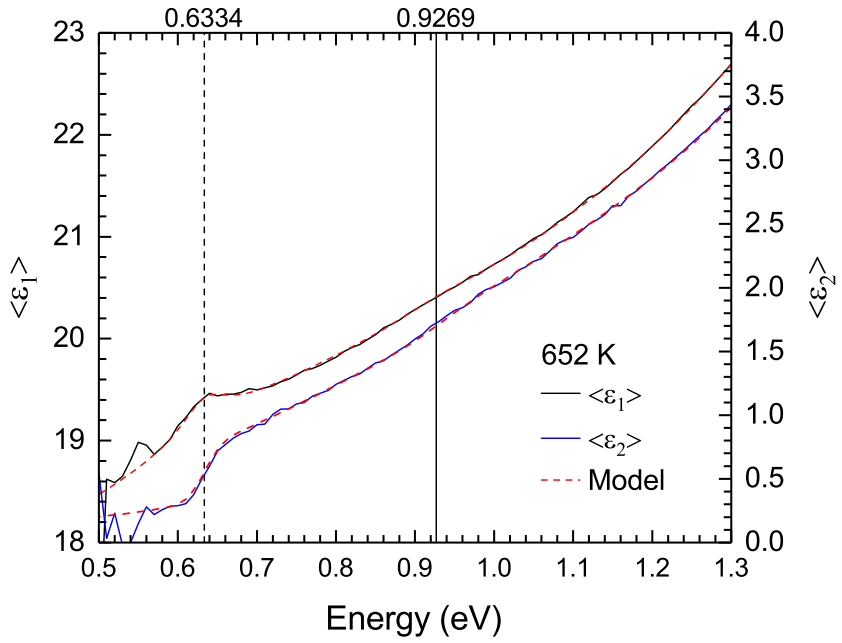

Figure 22: Infrared measurement: Critical points E_0 and $E_0 + \Delta_0$ at 652 K. The vertical lines indicate the critical point energies of E_0 (dash-dotted) and $E_0 + \Delta_0$ (solid) obtained by a parametric oscillator fit. For energies below about 0.6 eV the data starts to become noisy.

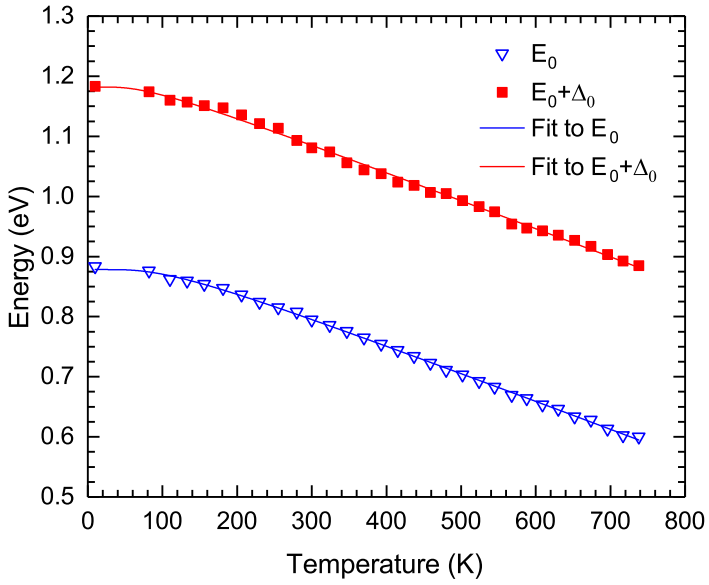

Figure 23: Temperature dependence of the E_0 ($\bigtriangledown$) and $E_0+\Delta_0$(■) critical point energies of bulk Ge. The energies have been determined using a parametric oscillator model. Fit to the data (solid lines) using the Bose-Einstein occupation factor described in equation (22).

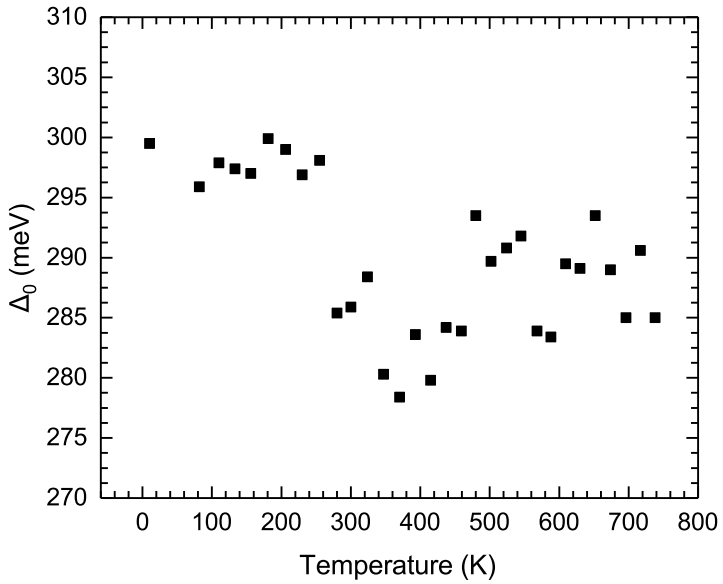

Figure 24: Energy difference Δ_0 between the E_0 and $E_0 + \Delta_0$ critical point energies of bulk Ge due to spin-orbit splitting.

the E_0 and $E_0 + \Delta_0$ critical points is observed. This temperature dependence of the E_0 and $E_0 + \Delta_0$ critical point energies can also be seen in figure 23, which shows the energies determined by using the parametric oscillator model. The fit to the data has been calculated using equation (22), the corresponding parameters can be found in table 1.

The spin-orbit splitting Δ_0, which approximately fluctuates between 278 meV and 300 meV, is supposed to be temperature independent. In fact, as can be seen in figure 10, a slight deviation at lower temperatures is observed. This might be due to an error in fitting the data and has to be determined and further analyzed.

It also has to be noted that the analysis of the critical points E_0 and $E_0 + \Delta_0$ using the second derivative method as described above and which was used for the other critical points does not provide reasonable data for the broadening of E_0 and $E_0 + \Delta_0$. The broadening calculated by this analysis method is smaller than the resolution $\Delta E = 2.5\ meV$ of the instrument. Also, excitonic effects have not been taken into account so far, but could be considered using the Tanguy model. Further analysis will be necessary to find the E_0 and $E_0 + \Delta_0$ critical point parameters and excitonic effects.

The two detectors were switched at an energy of 1.181 eV. This switch is visible in our data. It does not affect the analysis for the measurements at temperatures of 82 K and higher, but it is significant for the $E_0 + \Delta_0$ critical point at 10 K because at that temperature the energy of $E_0 + \Delta_0$ is found to be approximately 1.18 eV. It was possible to remove the step from the measured data afterwards so that the critical point after all can be resolved as is shown in figure 23, where the step has been removed. At the higher temperatures, the step is still visible, but does not the critical points since they are shifted to lower energies. In addition, very small steps due to the gratings changes described in the experimental section were obtained. Fortunately, the magnitude of these steps was low enough to be neglected since it had no influence on the analysis of the data.

6 Conclusion and Outlook

The measurement of the dielectric function of germanium (Ge) for different temperatures over a broad spectral range delivered valuable results. It was possible to investigate the critical point E_0 which occurs at the indirect band gap energy of Ge. At low temperatures we were even able to measure the very low peak corresponding to the $E_0+\Delta_0$ critical point, where Δ_0 is the spin-orbit splitting at the Γ-point of the Brillouin zone. For these low temperatures we used small step sizes of 0.5 meV, 1 meV and 2 meV together with a slit width of 1 mm which made it possible to resolve the very narrow and small peaks regarding to E_0 and $E_0+\Delta_0$.

The analysis of the critical points E_1, $E_1+\Delta_1$ and E_2 provided values which are in agreement with literature [1] [3]. For all critical points a temperature dependent energy shift was observed. This red-shift has two main contributions, one coming from thermal expansion and the other one from renormalization of energies due to electron-phonon interaction [1]. Also for the E_0 and $E_0+\Delta_0$ critical points a shift to lower energies for increasing temperature could be found. The temperature dependence of the E_0 and $E_0+\Delta_0$ critical point energies can be described in the same way as for the other critical point via an expression using the Bose-Einstein occupation factor.

As the E_0 and $E_0+\Delta_0$ peaks show a very small broadening and amplitude, the commonly used method to find the critical point parameters by analyzing the second derivative of the dielectric function did not deliver reasonable results. Therefore, a more precise method has to be applied. By calculating the Fourier coefficients and removing endpoint discontinuities of a chosen segment containing the E_0 and $E_0+\Delta_0$ critical points, it should be possible to find the energies, the broadenings and amplitudes.

Acknowledgements

My deepest gratitude goes to my thesis advisor Prof. Kurt Hingerl, who recommended me for this research period, and to Dr. Stefan Zollner, who was my supervisor at the New Mexico State University.

The research stay was fully successful, not only with respect to the valuable results of our measurements. To work in another physics lab was of great benefit for me, because I could gather precious knowledge in using spectroscopic ellipsometry and in analyzing ellipsometric data. I really profited from the extensive knowledge of Dr. Zollner and the other students working in his group and I am very thankful for that.

This four-month research period would not have been possible without financial support. Therefore, I want to thank the Austrian Marshall Plan Foundation as well as the Johannes Kepler University for their great support.

References

[1] L Vina, S Logothetidis, and M Cardona. Temperature dependence of the dielectric function of germanium. *Physical Review B*, 30(4):1979, 1984.

[2] P Lautenschlager, PB Allen, and M Cardona. Temperature dependence of band gaps in si and ge. *Physical Review B*, 31(4):2163, 1985.

[3] Nalin S Fernando, T Nathan Nunley, Ayana Ghosh, Cayla M Nelson, Jacqueline A Cooke, Amber A Medina, Stefan Zollner, Chi Xu, Jose Menendez, and John Kouvetakis. Temperature dependence of the interband critical points of bulk Ge and strained Ge on Si. *Applied Surface Science*, 2016.

[4] J.A. Woollam Co., Inc. Guide to using WVASE32.

[5] M. Cardona P. Y. Yu. *Fundamentals of Semiconductors*. Springer, 2010.

[6] J.A. Woollam Co., Inc., Lincoln, NE. Model V-VASE.

[7] Timothy Nathan Nunley, Nalin S Fernando, Nuwanjula Samarasingha, Jaime M Moya, Cayla M Nelson, Amber A Medina, and Stefan Zollner. Optical constants of germanium and thermally grown germanium dioxide from 0.5 to 6.6 ev via a multisample ellipsometry investigation. *Journal of Vacuum Science & Technology B, Nanotechnology and Microelectronics: Materials, Processing, Measurement, and Phenomena*, 34(6):061205, 2016.

[8] Richard C. Powell. *Symmetry, Group Theory, and the Physical Properties of Crystals*. Springer, 2010.

[9] J. F. Nye. *Physical Properties of Crystals*. Oxford University Press, 1985.

[10] N.M. Bashara R.M.A. Azzam. *Ellipsometry and Polarized Light*. Elsevier science B.V., 1987.

[11] Yatendra Pal Varshni. Temperature dependence of the energy gap in semiconductors. *physica*, 34(1):149–154, 1967.

[12] David E Aspnes and AA Studna. Dielectric functions and optical parameters of si, ge, gap, gaas, gasb, inp, inas, and insb from 1.5 to 6.0 ev. *Physical review B*, 27(2):985, 1983.

[13] P Lautenschlager, M Garriga, S Logothetidis, and M Cardona. Interband critical points of gaas and their temperature dependence. *Physical Review B*, 35(17):9174, 1987.

[14] P Lautenschlager, M Garriga, L Vina, and M Cardona. Temperature dependence of the dielectric function and interband critical points in silicon. *Physical Review B*, 36(9):4821, 1987.

[15] Cayla Marie Nelson, Maria Spies, Lina S Abdallah, Stefan Zollner, Yun Xu, and Hongmei Luo. Dielectric function of laalo3 from 0.8 to 6 ev between 77 and 700 k. *Journal of Vacuum Science & Technology A: Vacuum, Surfaces, and Films*, 30(6):061404, 2012.